ARMY RESEARCH LABORATORY

Comparison of Anisotropic versus Isotropic Metamaterials in Low Profile UHF Antenna Design

by Gregory A. Mitchell

ARL-TR-7012 **August 2014**

NOTICES

Disclaimers

The findings in this report are not to be construed as an official Department of the Army position unless so designated by other authorized documents.

Citation of manufacturer's or trade names does not constitute an official endorsement or approval of the use thereof.

Destroy this report when it is no longer needed. Do not return it to the originator.

Army Research Laboratory
Adelphi, MD 20783-1197

ARL-TR-7012 **August 2014**

Comparison of Anisotropic versus Isotropic Metamaterials in Low Profile UHF Antenna Design

Gregory A. Mitchell
Sensors and Electron Devices Directorate, ARL

REPORT DOCUMENTATION PAGE	Form Approved OMB No. 0704-0188

1. REPORT DATE *(DD-MM-YYYY)*	2. REPORT TYPE	3. DATES COVERED (From - To)
August 2014	Final	5/2013 to 2/2014

4. TITLE AND SUBTITLE

Comparison of Anisotropic versus Isotropic Metamaterials in Low Profile UHF Antenna Design

5a. CONTRACT NUMBER

5b. GRANT NUMBER

5c. PROGRAM ELEMENT NUMBER

6. AUTHOR(S)

Gregory A. Mitchell

5d. PROJECT NUMBER

5e. TASK NUMBER

5f. WORK UNIT NUMBER

7. PERFORMING ORGANIZATION NAME(S) AND ADDRESS(ES)

U.S. Army Research Laboratory
ATTN: RDRL-SER-M
2800 Powder Mill Road
Adelphi, MD 20783-1197

8. PERFORMING ORGANIZATION REPORT NUMBER

ARL-TR-7012

9. SPONSORING/MONITORING AGENCY NAME(S) AND ADDRESS(ES)

10. SPONSOR/MONITOR'S ACRONYM(S)

11. SPONSOR/MONITOR'S REPORT NUMBER(S)

12. DISTRIBUTION/AVAILABILITY STATEMENT

Approved for public release; distribution unlimited.

13. SUPPLEMENTARY NOTES

14. ABSTRACT

This report compares the use of anisotropic material versus isotropic material in a partially loaded cavity-backed antenna. Both magnetic and dielectric materials are studied, and a full case study is performed highlighting the different effects produced by varying the individual anisotropic tensor elements. The final result of the study is a design for a low profile (0.055λ) cavity backed antenna. The shape of the cavity is uniquely determined by a transverse resonance resulting from the partial loading and the permittivity and/or permeability of the anisotropic material. The performance of the final design compares favorably both in realized gain and VSWR from 300 MHz–500 MHz to a benchmark case. The benchmark case has the same aperture dimensions, but a large profile ($.275\lambda$) due to the absence of the high index anisotropic material.

15. SUBJECT TERMS

16. SECURITY CLASSIFICATION OF:			17. LIMITATION OF ABSTRACT	18. NUMBER OF PAGES	19a. NAME OF RESPONSIBLE PERSON
A. Report	b. ABSTRACT	c. THIS PAGE			Gregory A. Mitchell
Unclassified	Unclassified	Unclassified	UU	38	19b. TELEPHONE NUMBER (*Include area code*) (301) 394-2322

Contents

List of Figures

List of Tables

INTENTIONALLY LEFT BLANK.

1. Introduction

Resonating cavities have been used as a means to achieve stable and unidirectional radiation patterns for mounted antenna apertures. Radiation properties such as resonant frequency (f_r) and realized gain are directly determined by the rectangular cavity dimensions. Generally, the f_r is defined by the half-free space wavelength at the desired frequency, while best gain results occur for a quarter-wavelength rectangular cavity in the normal direction.

Many applications in wireless communications and radar require antennas that conform to the surface of the supporting structure. Whenever applicable, the antenna aperture is approximated by a flat plane with the requirement that the dimension normal to the aperture ("profile") be minimized. Low profile antennas are of special importance within the UHF band, where they are used as communications antennas on military platforms. Low profile antennas reduce platform visibility and decrease antenna weight, which becomes critically important in airborne platforms. In addition, many military vehicles contain several protruding antennas for multiple communication links at UHF frequencies. Therefore, there is great interest in developing low profile antennas with wide bandwidths (BW). Meeting both requirements at the long wavelengths involved poses special difficulties. Although the subject of profile reduction for flush-mounted antennas is not new, the number of papers dealing specifically with UHF band designs is surprisingly small. Two recently proposed designs employ variants of a discone antenna (*1*–*3*).

Traditionally, magnetic materials have high losses at microwave frequencies above 100 MHz, which makes them unsuitable as substrates for UHF antenna structures. The availability of artificial magnetic metamaterials has widened the range of possible design approaches. Of particular interest are high index magnetic materials ($\mu_r \geq 10$) that exhibit low loss in the UHF band (*4*–*5*). Furthermore, the development of artificial magnetic metamaterials allows engineers to separately control the values of both magnetic permeability and electric permittivity. Preliminary research results documented in this report show that anisotropic magnetic metamaterials give superior performance to isotropic magnetic or dielectric materials, even when low losses are assumed for all cases.

The goal of this report is to analyze the properties of high index anisotropic magnetic metamaterials as an effective material used to load a low profile UHF antenna (LPA) backed by a rectangular cavity. Traditionally, rectangular cavity-backed apertures require an electrical height of $\lambda_g/4$—resulting in a large profile at UHF frequencies, as λ_g becomes very large. By loading the rectangular cavity with high index material ($\sqrt{\mu_r \varepsilon_r}$), the size of λ_g is reduced, thereby reducing the height of the antenna's profile. This report presents research results of an antenna model where the profile reduction is achieved with high index artificial magnetic

metamaterials. The antenna under investigation is a flanged rectangular aperture backed by a tapered rectangular cavity, terminated by a short circuit. An appropriately shaped high index magneto-dielectric material within the cavity establishes local resonance conditions with the inner conducting walls. Further, this report demonstrates that using anisotropic magnetic metamaterials to load this cavity achieves positive realized gain from 220 MHz–555 MHz with a cavity profile depth of $0.055\lambda_r$, where λ_r is the cutoff free-space wavelength based on the dimensions of the aperture.

2. Sub-Wavelength Cavities Loaded with High Index Materials

This section details an extensive case study of the effects of loading a rectangular cavity with high index materials. Both dielectric and magnetic materials are investigated. The case study demonstrates the effects that high index materials have on the reduction of the antenna profile compared to an antenna of the same dimensions with an air-filled rectangular cavity. Comparisons of the antenna's performance—in terms of input impedance match and far field realized gain—to that of a traditional air-filled cavity are discussed in terms of the tradeoffs in antenna performance versus the reduction of the antenna profile at UHF frequencies. All materials in this report are assumed to be lossless, and the figures of merit used are the far field realized gain, S11, and/or VSWR of the antenna. All simulations have been run using the time domain solver of CST Studio Suite 2013, and adaptive meshing has been used to verify convergence in the far field results.

2.1 Air Filled Rectangular Cavity Benchmark Antenna

The first step in the course of this investigation was to provide a benchmark for antenna performance. This section illustrates the design and simulation of a rectangular cavity-backed antenna with a rectangular aperture and a resonant frequency of f_r = 200 MHz, where f_r is defined as

$$f_r\left(MHz\right) = \frac{c_o}{1x10^6 \lambda_o \sqrt{\varepsilon_r \mu_r}}, \tag{1}$$

and represents the lowest frequency, which allows the first resonance for the given cavity dimensions (*6, 7*).

The antenna is optimized for performance based on the realized gain and VSWR of the model, and does not take the profile of the antenna into account. This results in an antenna that performs well, but has a large profile.

A coaxial feed has long been used to stimulate electric and magnetic fields within a rectangular waveguide. This coaxial-to-waveguide junction has been widely studied, and many successful

methods have been developed. Generally, a coaxial input is fed into the center of the widest transverse waveguide dimension, and a conducting probe is used to stimulate the field within the rectangular waveguide (*8*, *9*). We will use similar feeding techniques to attempt to achieve a broadband match for an open rectangular cavity surrounded by an infinite flange; however, the probe will be placed close to the aperture.

Figure 1a shows the layout of the air-filled rectangular cavity, while figure 1b shows the 3D view of the CST model used for the simulation. Table 1 shows the dimensions used to generate the results of figures 2a and 2b. The size of the aperture is designed to be $a = \lambda_o/2$ at 200 MHz, and the back short = 10.2 in corresponds to $0.275\lambda_r$ at the center frequency (350 MHz) of the frequency band of interest where

$$\lambda_r = \frac{\lambda_o^{cf}}{\sqrt{0.5\varepsilon_r\mu_r - \left(\frac{\lambda_o^{cf}}{(2a)}\right)^2}}, \tag{2}$$

λ_o^{cf} is the free space wavelength at the center frequency, and λ_r is the average resonant wavelength inside the cavity at $z = d/2$. The width (PW) and length (L) of the probe have been optimized to provide the best impedance match at the coaxial input.

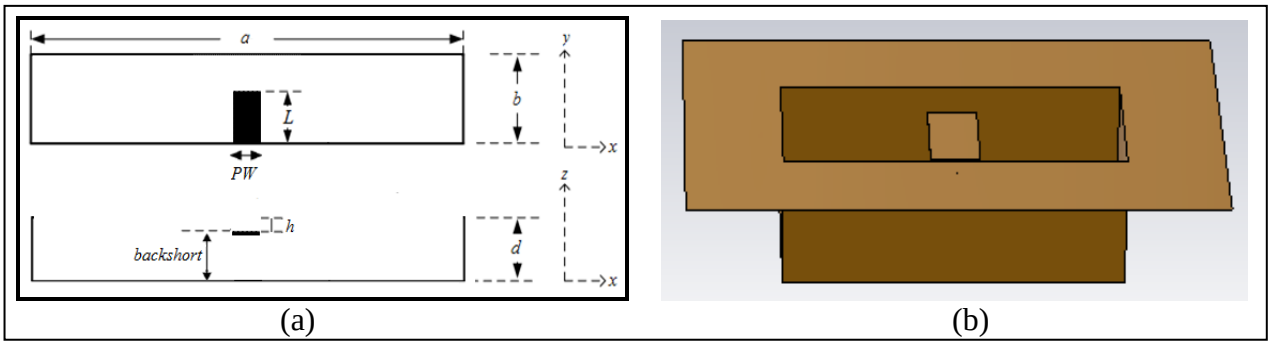

Figure 1. Illustration of (a) the geometry of the rectangular cavity backed rectangular aperture and cylindrical probe feed and (b) three dimensional view of the CST model.

Table 1. Dimensions in inches for the simulations run for geometry in figures 1a and 1b.

back short	***a***	***b***	f_r **(MHz)**	***PW***	***L***	***h***	***d***
10.2	29.5	13.1	200	4.3	8.5	0.84	11.04

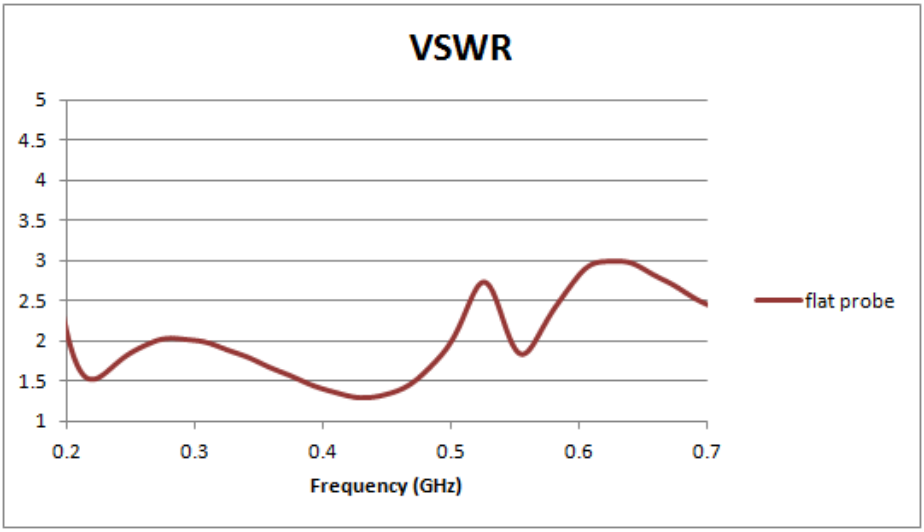

(a)

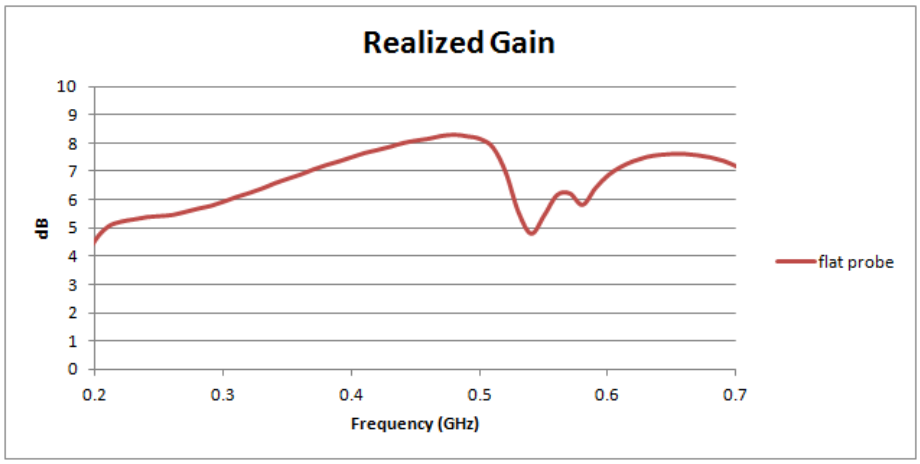

(b)

Figure 2. Simulation results of the model in figure 1a and 1b for (a) VSWR and (b) realized gain.

Figures 2a and 2b show a VSWR of 3:1 or better from 200 MHz–700 MHz, with a realized gain ranging from 5–8 dB. Since this design uses an air-filled rectangular cavity, the total profile of the antenna remains much too large, with d = 11.04 in. The next section investigates how loading the rectangular cavity with high index material serves to reduce the profile of the antenna.

2.2 Rectangular Cavity Loaded with High Index Material

Section 2.1 provided a suitable benchmark to compare against all iterations of the LPA design. While the performance of the benchmark antenna was very good in terms of VSWR and realized gain, the 11.04 in profile needs to be reduced by more than 75% to achieve an adequate LPA design. This section shows how loading the antenna from section 2.1 with high index material reduces the rectangular cavity profile.

Equation 2 indicates that by increasing ε_r and/or μ_r, the value of λ_r is reduced, which will serve to reduce the profile of the rectangular cavity since this is approximately $\lambda_r/4$ at 350 MHz. Figures 3a and 3b show a rectangular cavity loaded with a high index dielectric material with $\mu_r = 1$ and $\varepsilon_r = 10$.

Table 2 shows the dimensions of this initial LPA design. The transverse dimensions (a and b) of the aperture and rectangular cavity remain the same, as do the dimensions of the probe (*PW* and *L*); however, the introduction of the dielectric material has reduced the profile of the antenna to 3.11 in, or $0.053\lambda_r$, from 11.04 in. This demonstrates the ability to significantly reduce the profile of the antenna by loading the rectangular cavity with a high index material.

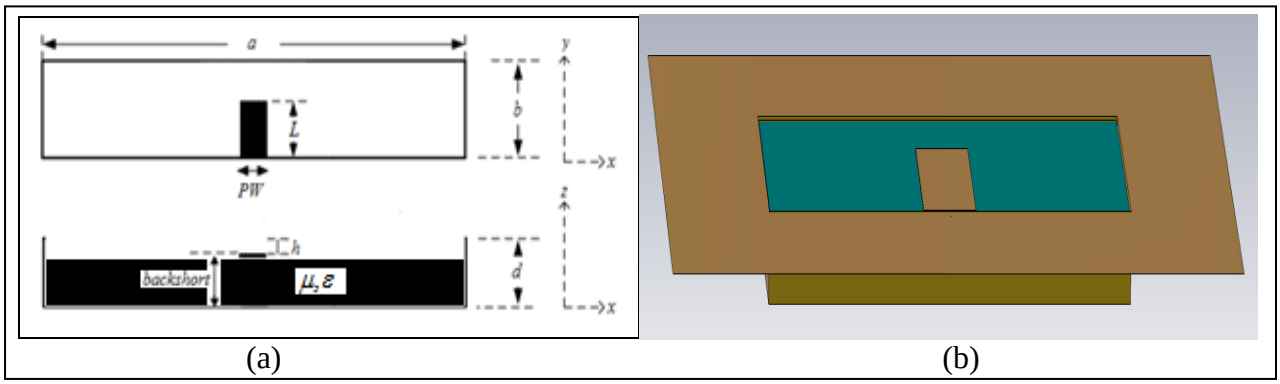

Figure 3. Illustration of (a) the geometry of the rectangular cavity backed rectangular aperture loaded with high index material and (b) three dimensional view of the CST model.

Table 2. Dimensions in inches for the simulations run for geometry in figure 3a and 3b.

back short	***a***	***b***	f_r **(MHz)**	***PW***	***d***	***L***	***h***
2.98	29.5	13.1	200	4.3	3.11	8.5	0.12 (3.125 mm)

Figures 4a and 4b show the VSWR and realized gain for the LPA design depicted in figures 3a and 3b. The unstable nature of the VSWR indicates that there are several resonances operating within the rectangular cavity for these dimensions—which is expected because equation 1 says that when μ_r and/or ε_r of the material inside the rectangular cavity increases, f_r decreases.

For the benchmark antenna in section 2.1 ($\varepsilon_r = 1$, $\mu_r = 1$, and $a = 29.5$"), the VSWR and realized gain of figures 2a and 2b show stable results. For the LPA depicted in figures 3a and 3b ($\varepsilon_r = 10$, $\mu_r = 1$, and $a = 29.5$"), $f_r = 63.25$ MHz yielding unstable results for the VSWR and realized gain of figures 4a and 4b. Since additional resonances begin to operate at each octave, this means that every 63.25 MHz an additional resonance is introduced to the rectangular cavity so that at 200 MHz there are up to three resonances operating inside the rectangular cavity, and at 500 MHz there are as many as seven resonances.

The results of figures 4a and 4b show that as more resonances begin to appear within the rectangular cavity, the performance of the LPA is severely degraded. Since reducing the profile

of the benchmark antenna requires the use of high index materials, the next step is to determine a novel way to suppress these higher order resonances and maintain a constant f_r, even when the rectangular cavity is loaded with high index materials.

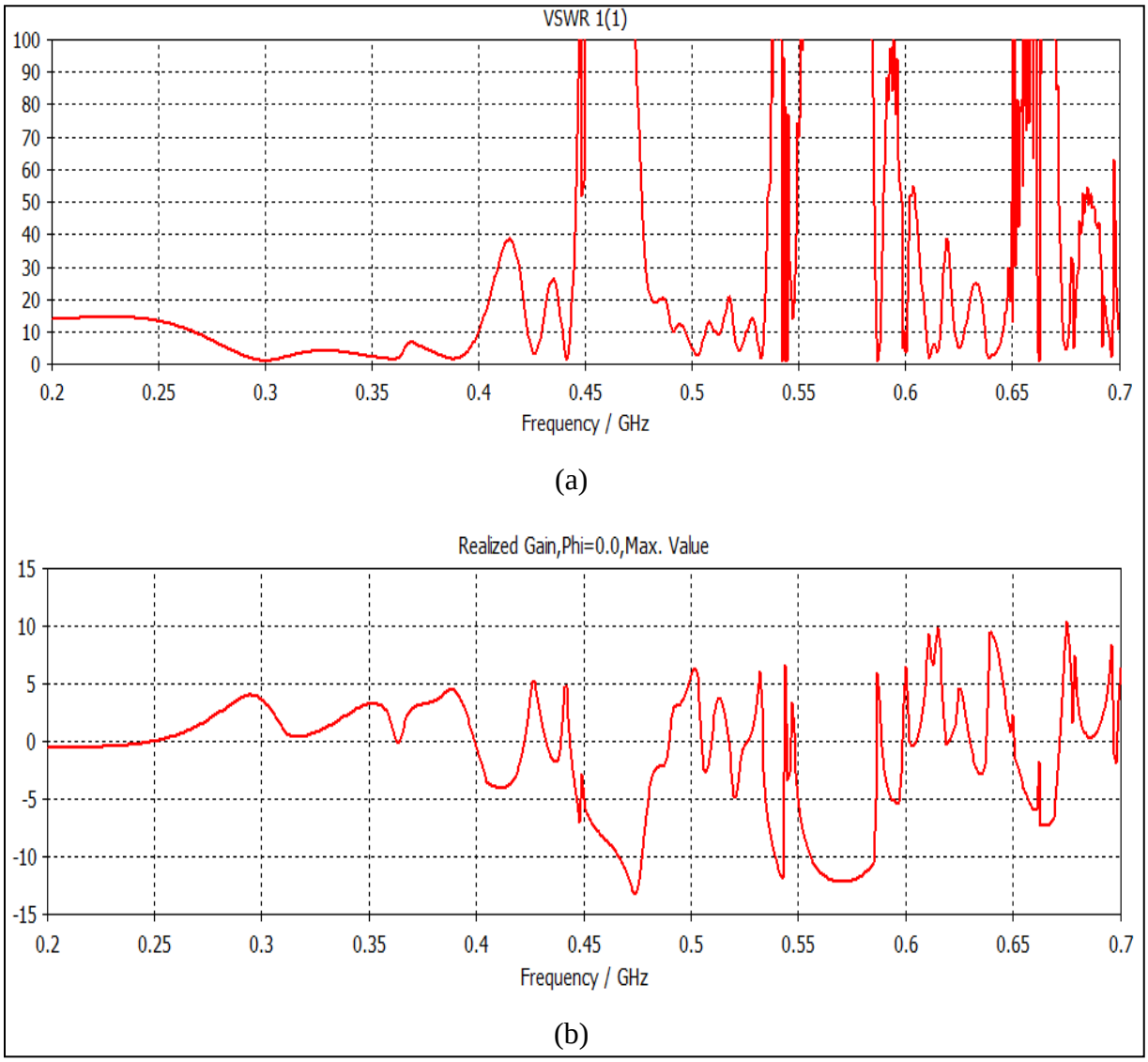

Figure 4. Simulations of the model in figures 3a and 3b of the rectangular cavity loaded with high index dielectric for (a) VSWR and (b) realized gain.

2.3 Suppression of Higher Order Resonances in a Loaded Rectangular Cavity

Section 2.2 shows that in a rectangular cavity the appearance of higher order resonances will serve to increase the instability in VSWR and realized gain. Therefore, only the first resonance should operate over the frequency band because multiple resonances tend to interfere destructively. The resonant frequency, f_r, needs to remain constant to ensure operation of only the lowest resonance at the frequency of operation.

Figures 5a and 5b show the geometry of a partially loaded rectangular cavity that has been linearly tapered in such a way as to maintain a nearly constant f_r. Note that the high index material is also linearly tapered using an inverse relationship to that of the width of the rectangular cavity walls. Here, $a_0 = \lambda_r/2$, $a_1 = \lambda_r / (2\sqrt{\mu_r \varepsilon_r})$, and $a(z) \approx \lambda_r(z)/2$ where $\lambda_r(z)$ changes to maintain f_r dependent on the width of the high index material at point z. In this model, a_0 serves the same purpose as rectangular cavity dimension a served in sections 2.1–2.2, where f_r = 200 MHz and w = 0 in. Dimension a_1 represents the value of $\lambda_r/2$ that maintains f_r = 200 MHz when the transverse plane of the rectangular cavity is completely filled with high index material and $w = \dfrac{\lambda_r}{2\sqrt{\varepsilon_r \mu_r}}$. The shape of the rectangular cavity is determined by a straight line between these two points. This is only an initial approximation to the shape of the rectangular cavity, but by investigating how this approximation works, a determination can be made whether this type of model for the LPA is worth pursuing.

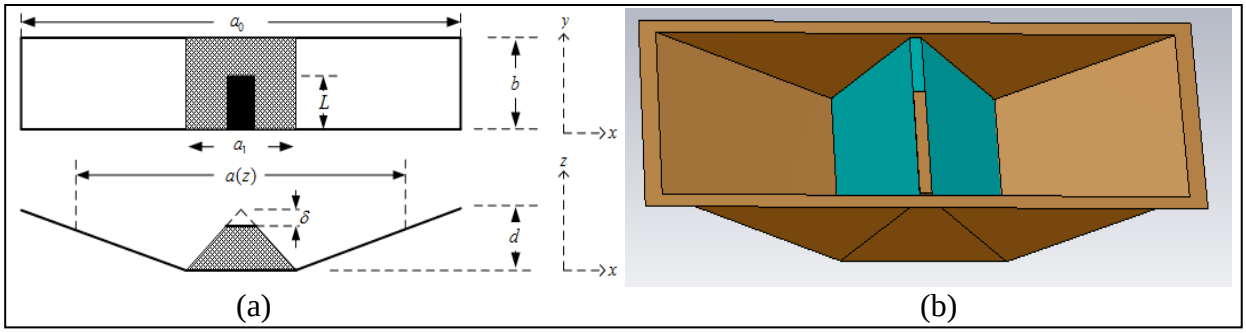

Figure 5. Illustration of (a) the geometry of a tapered rectangular cavity partially loaded with high index material and (b) three dimensional view of the CST model.

The profile height d is determined as $\lambda'_r/4$ where for the geometry shown in figure λ'_r is

$$\lambda'_r = \frac{\lambda_o^{cf}}{\sqrt{0.5\varepsilon_r \mu_r - \left(\dfrac{\lambda_o^{cf}}{(a_0 + a_1)}\right)^2}} . \qquad (3)$$

Equation 3 averages λ_r from equation 2 over d for the changing ratio of high index material to air in the cavity. The quantity δ is the distance between the top of the high index material and the antenna aperture. Ideally, the material would end in a tip with infinitesimal width, but this type of structure cannot be resolved in a numerical model. The next step in the design of the LPA will be to analyze whether the design described in this section allows for significant profile reduction without causing the instabilities seen in figures 4a and 4b.

2.4 Linearly Tapered Rectangular Cavity Loaded with Isotropic Material

Section 2.3 described an idea for suppressing the high order resonances within a rectangular cavity, even when loaded with high index materials. This section examines the antenna design

theorized in section 2.3 when the rectangular cavity is loaded with isotropic high index materials that exhibit dielectric and/or magnetic properties. The hope is to see a significant reduction in antenna profile from the benchmark antenna from section 2.1, while achieving positive realized gain from 200 MHz–500 MHz.

Table 3 gives the dimensions corresponding to figure 5a for the antenna models analyzed in this section. The f_r has been reduced to 192.5 MHz because the behavior in a rectangular cavity can be unpredictable directly at the cutoff f_r. In practice it is usually best to lower f_r to a value just below the desired frequency. PW has been reduced to be the same width as the top of the dielectric material. This was initially thought to provide the smoothest impedance transition from the high index material to free space.

Table 3. Dimensions in inches for the simulations run for the geometry in figure 5a and 5b.

a_0	b	a_1	f_r (MHz)	d	δ	PW	L
30.68	13.64	9.7	192.5	4.1	0.27	0.7	8.5

Immediately, figures 6a and 6b show relative stability of the realized gain and S11 curves, which indicates that the model described in section 2.3 has successfully suppressed the high order resonances that caused the instabilities at the higher end of the frequency band. The rest of this section will be dedicated to explaining the difference in how dielectric, magnetic, and magneto-dielectric materials affect the LPA's performance.

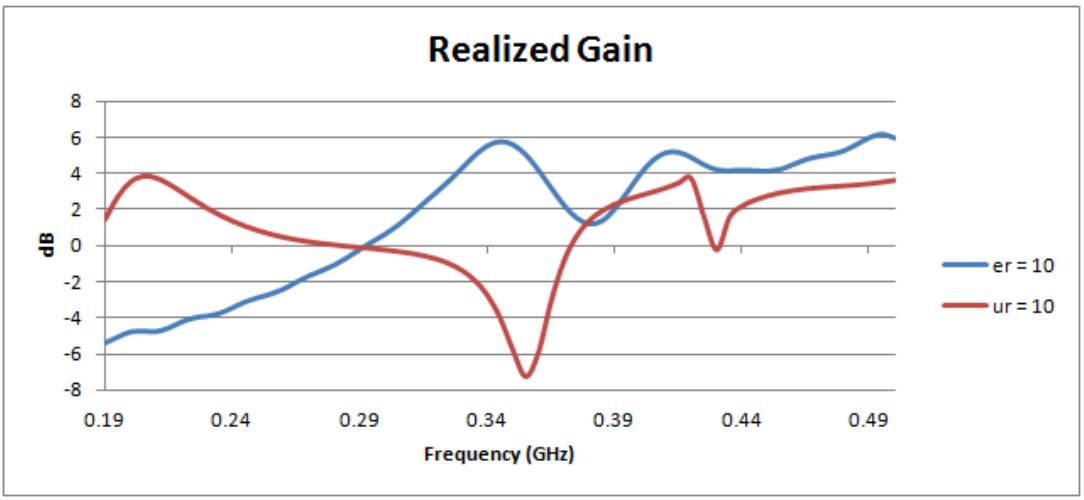

(a)

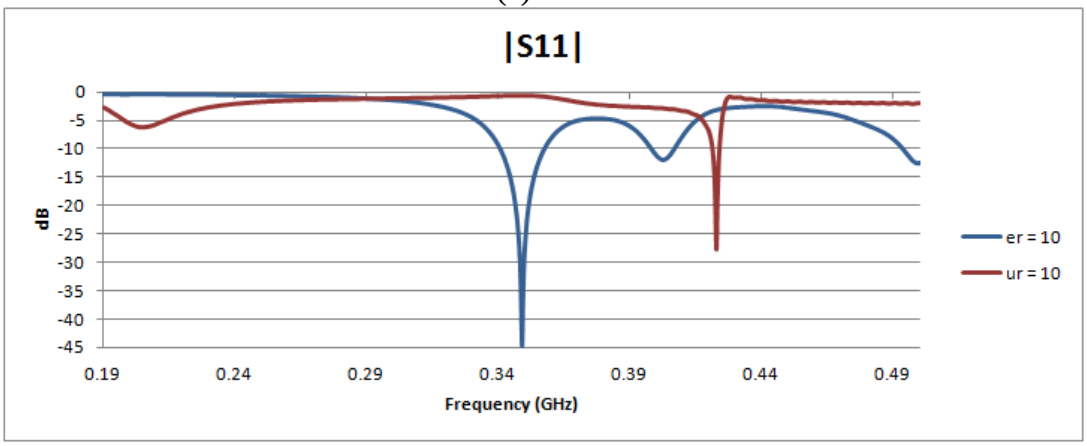

(b)

Figure 6. Simulation results for the LPA model in figure 5a loaded with dielectric and magnetic isotropic material for (a) realized gain and (b) S11.

Figures 6a and 6b show the realized gain and S11 curves for isotropic materials with values of ε_r = 10 and μ_r = 1, as well as ε_r = 1 and μ_r =10, respectively for a LPA with the dimensions listed in table 3. Based on equation 3, a profile of d = 4.1 in, or 0.07λ_r for f_r = 192.5 MHz, has been achieved compared to d = 11.04 in or 0.19λ_r for the benchmark antenna design from section 2.1. The dimensions of a_0 and b yield an aperture size of 2.9 ft^2, discounting the infinite flange.

For the dielectric material, from 290 MHz–500 MHz there is a positive realized gain even though the S11 is not particularly good over the entire range. This stems from the fact that there is a large aperture of 2.9 ft^2, which becomes larger in terms of wavelength as frequency increases. At 350 MHz, where $d = \lambda'_g/4$, there is a narrowband match of better than –40 dB corresponding to the peak realized gain of about 5.8 dB. This is expected since the best performance occurs for the air-filled rectangular cavity when the back short is located approximately $\lambda_g/4$ from the aperture at the center frequency.

For the magnetic material, the realized gain starts out positive from 200 MHz and crosses 0 dB at the same point that the realized gain for the dielectric material becomes positive at 290 MHz. The realized gain becomes positive again at about 275 MHz. While both curves have a dip at 420 MHz, the dip of the magnetic material is much more pronounced and it also finishes much lower at the end of the frequency band. The S11 of the magnetic material shows extremely poor S11 over much of the band from 200 MHz–500 MHz. Since the dielectric material and magnetic material seem to cover different parts of the spectrum in terms of positive realized gain, it will be interesting to see how a magneto-dielectric material responds.

Figures 7a and 7b show the realized gain and S11 curves for an isotropic magneto-dielectric material with values of $\varepsilon_r = \sqrt{10}$ and $\mu_r = \sqrt{10}$, respectively. These values were chosen so that the antenna dimensions match those in table 3.

Figure 7a shows a realized gain pattern that has negative realized gain over much of the band from 200 MHz–420 MHz. This seems to indicate that using magneto-dielectric materials is not as effective as a purely magnetic or dielectric isotropic material. Decreasing the values of ε_r and μ_r until they approached unity would, in fact, trend the curve in figures 7a and 7b towards that of the benchmark antenna, but that goes against the reduction of the cavity profile.

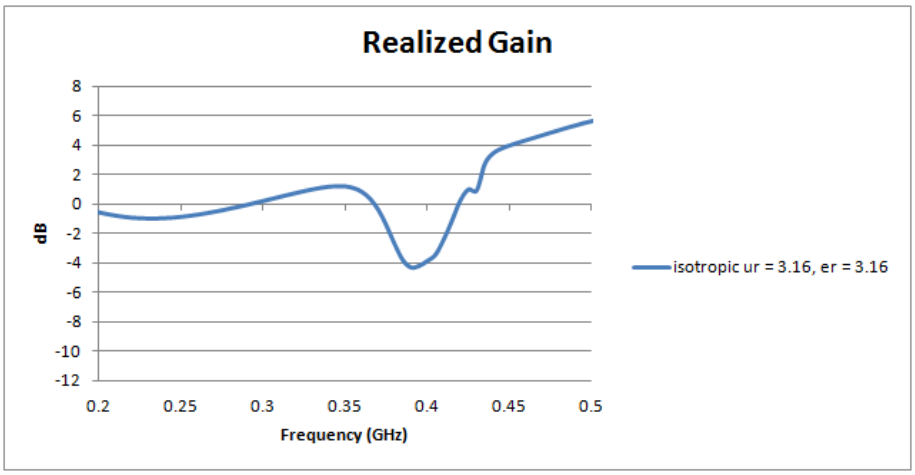

(a)

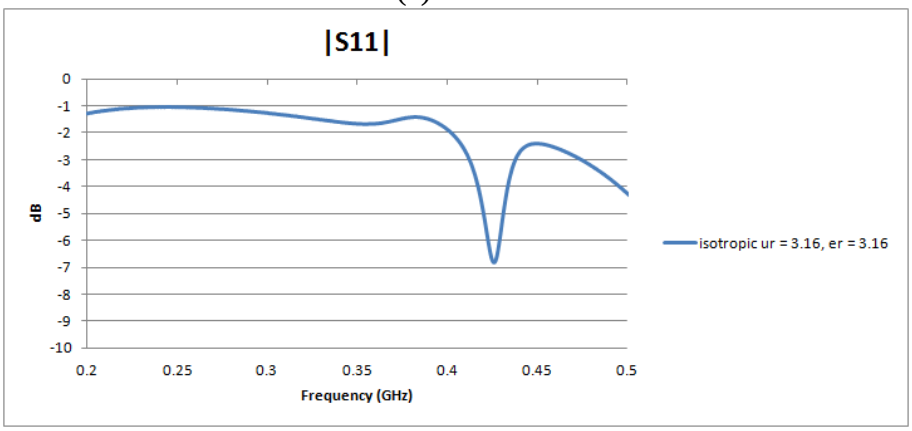

(b)

Figure 7. Simulation results for the LPA model in figure 5a loaded with magneto-dielectric isotropic material for (a) realized gain and (b) |S11|.

This section has demonstrated the ability to reduce the antenna profile by 63% with a partial loading of the benchmark antenna. A linearly tapered rectangular cavity and inversely tapered load successfully suppress the higher order resonances seen in the results of section 2.2. Both the cases for dielectric and magnetic material loads in this section have shown positive realized gain performance over parts of the frequency band; however, the design goals of positive realized gain over 200 MHz–500 MHz are not met for any of the cases analyzed thus far. The next step in the design of the LPA is to investigate whether anisotropic materials provide any improvement over isotropic materials for the same linearly tapered rectangular cavity design.

2.5 Linearly Tapered Rectangular Cavity Loaded with Anisotropic Material

Section 2.4 showed the potential to reduce the LPA profile at UHF frequencies by up to 63% and still produce a positive realized gain over parts of the band from 200 MHz–500 MHz. As seen from the isotropic materials, the differences between dielectric, magnetic, and magneto-dielectric materials cause a positive gain response in different areas of the frequency band. However, these LPA designs were not able to get a positive realized gain across the entire frequency band of

200 MHz–500 MHz for a low profile rectangular cavity requiring relatively high values of ε_r and/or μ_r. This section analyzes the effects that uniaxial anisotropic materials have on the performance of the antenna model described in section 2.3.

The anisotropy of the effective media is defined by the following two tensors:

$$\varepsilon_r = \begin{bmatrix} \varepsilon_x & 0 & 0 \\ 0 & \varepsilon_y & 0 \\ 0 & 0 & \varepsilon_z \end{bmatrix} \quad \text{and} \quad \mu_r = \begin{bmatrix} \mu_x & 0 & 0 \\ 0 & \mu_y & 0 \\ 0 & 0 & \mu_z \end{bmatrix}. \tag{4}$$

By isolating individual components of the permittivity and permeability tensors, hopefully behavior can be identified that, if exploited, will improve the S11 and realized gain curves over those of section 2.4 while still maintaining a profile of the same order.

This section examines how anisotropy in a single tensor element of equation 4 affects the behavior of the LPA design. All other tensor elements will be set to unity in each case. I will refer to the axis of analysis as the dominant axis. The same form of equation 3 will be used where ε_r and μ_r will be replaced with the tensor values of the dominant axis.

Figures 8a and 8b show the realized gain and S11 for an LPA with dimensions listed in table 3. The linearly tapered cavity is loaded with an anisotropic medium with $\varepsilon_x = 10$, $\varepsilon_y = 10$, or $\varepsilon_z = 10$, respectively. The blue curve represents the $\varepsilon_x = 10$ case and clearly shows the best wideband performance in terms of positive realized gain from 240 MHz–920 MHz or a 283% BW. In this case, the dominant axis of the permittivity tensor is aligned in the same direction as the H-field at the aperture. The red curve shows the realized gain for the $\varepsilon_y = 10$ to be positive from about 215 MHz–605 MHz, or a 181% BW. In this instance, the dominant axis of the permittivity tensor is aligned in the same direction as the E-field at the aperture. Comparing the red and blue curves shows that the LPA performs better at a lower frequency by sacrificing about an octave of BW. The green curve represents the $\varepsilon_z = 10$ case and shows a positive realized gain from about 340 MHz–460 MHz, while it goes positive again from about 575 MHz–895 MHz. This is the narrowest band of positive realized gain seen in the frequency band of interest and does not warrant further investigation.

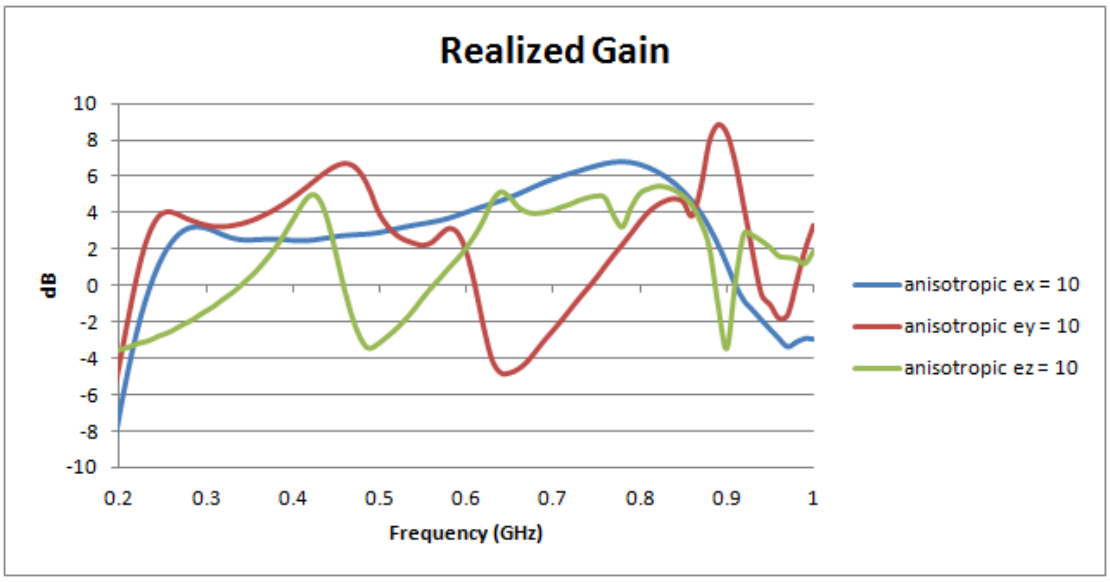

(a)

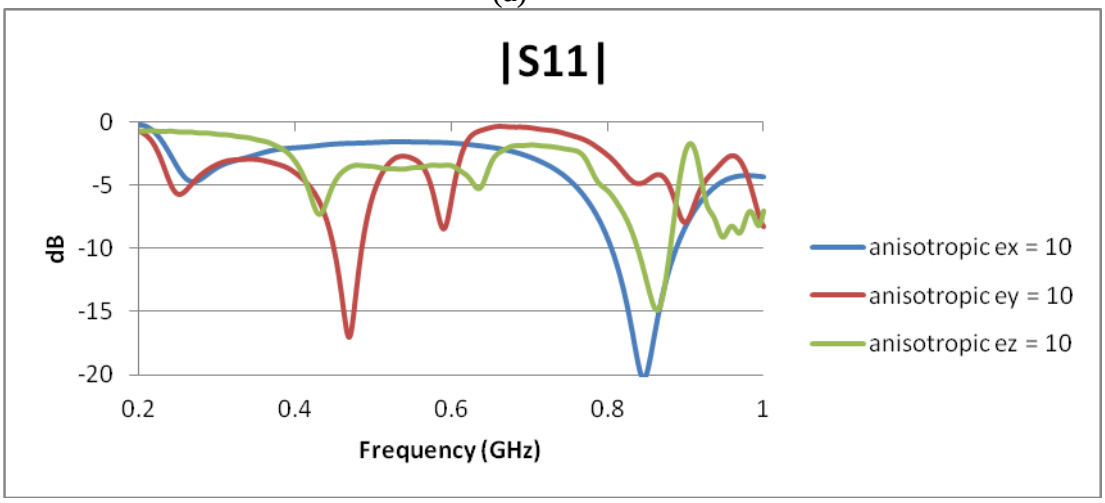

(b)

Figure 8. Simulation results of the model in figure 5a loaded with dielectric anisotropic material for (a) realized gain and (b) |S11|.

Figure 8b shows that these positive realized gains do not necessarily mean there is a good input impedance match. Even for a –2 dB value of S11, there can still be a positive realized gain. Again, this stems from the large size of the aperture in terms of wavelength, especially at the higher frequencies. However, a poor impedance match means much of the input power will be reflected, resulting in an inefficient antenna that wastes the bulk of the power supplied to it. Clearly, the wideband S11 curves need improvement to achieve the design goal of a 3:1 VSWR.

Figures 9a and 9b show the realized gain and S11 for a LPA with dimensions listed in table 4. The linearly tapered cavity is loaded with an anisotropic medium with $\mu_x = 10$, $\mu_y = 10$, or $\mu_z = 10$, respectively. The blue curve represents the $\mu_x = 10$ case for an antenna with the dimensions listed in table 4. In this instance, the dominant axis of the permeability tensor is in

the same direction as the H-field at the aperture. This case shows positive realized gain from 200 MHz–540 MHz. The curve shows promise that the BW of the positive realized gain can be increased 680 MHz by improving the impedance match from 525 MHz–550 MHz. The dimensions in table 4 also show that the size of the aperture has reduced to 2.1 ft^2, disregarding the flange from the 2.9 ft^2 of the previous cases. The reduction in aperture size, positive realized gain down to 200 MHz, and the potential for up to a 240% BW makes this case particularly interesting.

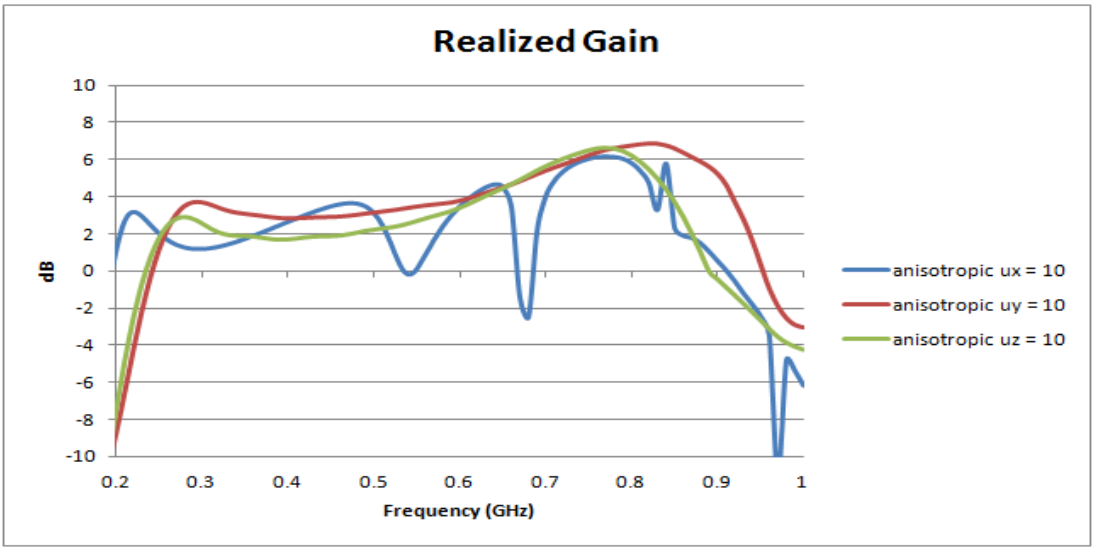

(a)

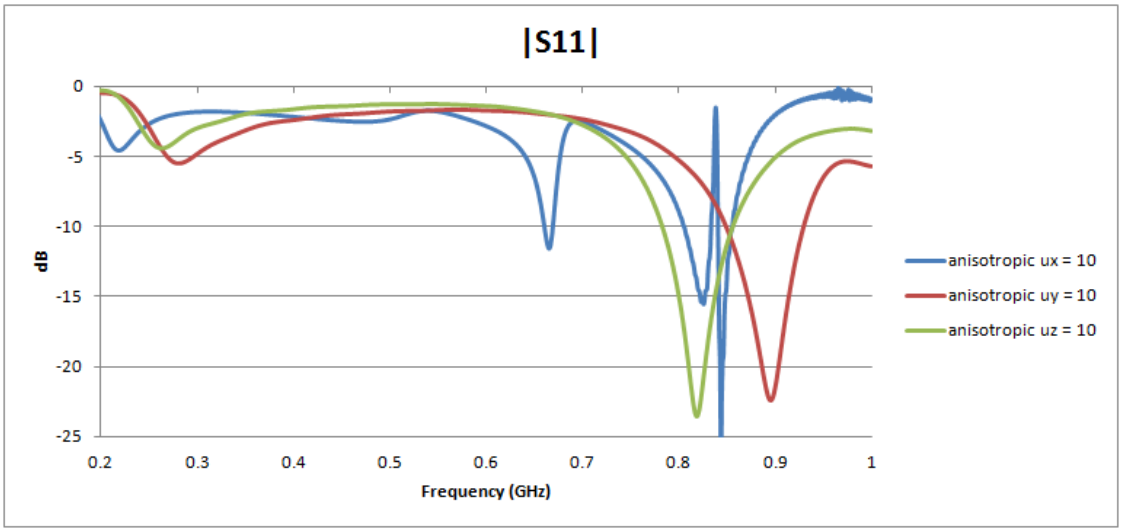

(b)

Figure 9. Simulation results of the design in figure 5a loaded with anisotropic magnetic material for (a) realized gain and (b) |S11|.

Table 4. Dimensions in inches for the $\mu_x = 10$ case corresponding to the geometry in figures 5a and 5b.

a_0	b	a_1	f_r (MHz)	d	δ	PW	L
26.25	11.7	8.3	225	4.2	0.27	0.7	8.5

The red curve represents the $\mu_y = 10$ case for an antenna with the dimensions listed in table 3. In this instance, the dominant axis of the permeability tensor is in the same direction as the E-field at the aperture. This case shows almost identical performance to the $\varepsilon_x = 10$ case with a 240 MHz–920 MHz or a 283% BW. The green curve represents the $\mu_z = 10$ case and shows similar behavior to the $\mu_y = 10$ case with a positive realized gain from about 240 MHz–895 MHz. However, it is less wideband and has a lower realized gain than the $\mu_y = 10$ case over the whole band. Again, figure 9b shows a flat S11 response, but the match needs to be improved across the entire band of interest in all three cases.

This section has demonstrated an improvement in the performance of the LPA design when loaded with anisotropic material versus when loaded with isotropic material. A realized gain has been demonstrated over the entire frequency band of interest for the $\mu_x = 10$ case. While this result is encouraging, the S11 curve shows how poor the input impedance match of this design is. However, as a preliminary design the potential to produce a positive realized gain for a LPA is there, and the results in this section indicate that using anisotropic material is advantageous over isotropic material in this design. Since the $\mu_x = 10$ case produces an LPA profile of $d = 4.1$ in, the next step in the design process is to determine whether further reduction of the LPA's profile is possible without degrading the performance any further. If further reduction in the LPA profile is possible, then the focus can shift to improving the S11 of the final LPA design.

2.6 Further Reduction in Cavity Profile Using Anisotropic Magnetic Material

Section 2.5 showed that the $\mu_x = 10$ anisotropic case is the only configuration to achieve a positive realized gain across the entire frequency band of interest. This makes it a prime candidate for increasing the value of μ_x to reduce the rectangular cavity profile d while potentially maintaining a positive realized gain.

Figures 10a and 10b show the realized gain and S11 for an anisotropic medium with $\mu_x = 10$ and $\mu_x = 15$, respectively. The blue curve corresponds to the $\mu_x = 10$ case with LPA dimensions listed in table 4, and the red curve corresponds to the $\mu_x = 15$ case with LPA dimensions listed in table 5. There is very little difference in the realized gain and S11 curves except for a slight shift down in frequency when $\mu_x = 15$. This means the potential BW has reduced from 240% to 215%, assuming the match is improved to bring the realized gain positive over the 500 MHz–520 MHz trough in the realized gain curve. This is an acceptable tradeoff because there is still a positive realized gain over the band from 200 MHz–500 MHz while reducing the profile of the LPA to $d = 3.29$ in, or $0.055\lambda_r$, compared to $d = 4.1$ in, or $0.07\lambda_r$, in section 2.5.

Table 5 gives the antenna dimensions for $\mu_x = 15$, with a rectangular cavity profile of d = 3.29 inches or $0.055\lambda_r$.

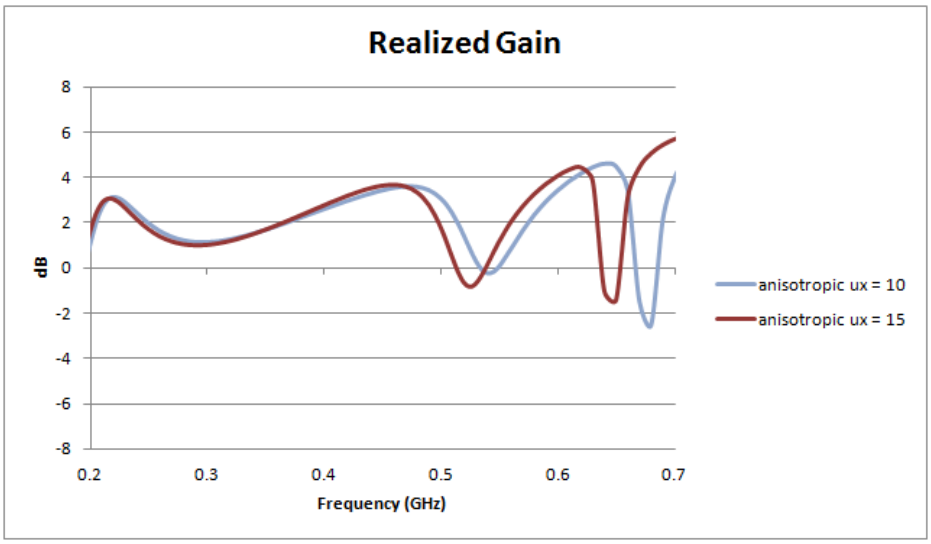

(a)

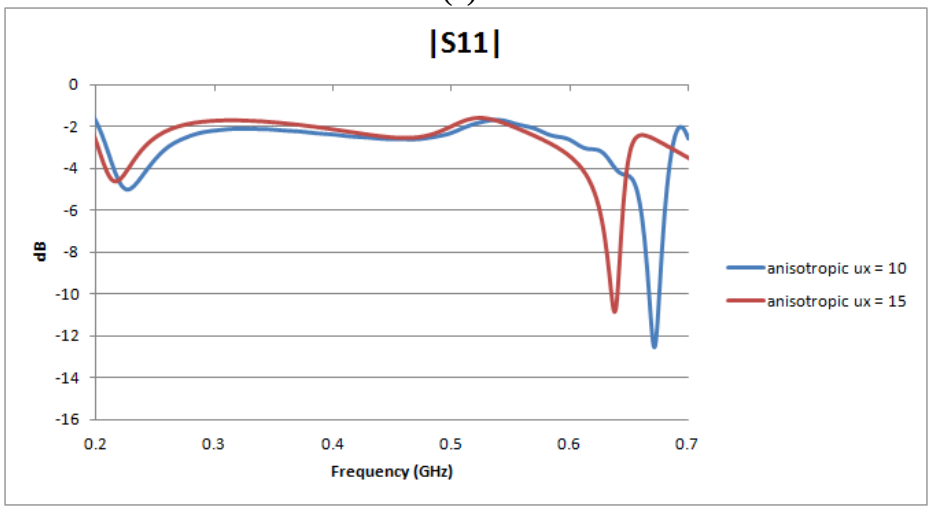

(b)

Figure 10. Simulation results of the model in figure 5a for anisotropic magnetic material with $\mu_x = 15$ for (a) realized gain and (b) |S11|.

Table 5. Dimensions in inches for the $\mu_x = 15$ case corresponding to the geometry of figure 5a and 5b.

a_0	b	a_1	f_r (MHz)	d	δ	PW	L
26.25	11.7	8.3	225	3.29	0.27	0.7	8.5

This section has demonstrated that increasing the permeability has the desired effect of further reduction in the LPA profile while having very little effect on the LPA's performance. This means that after improving the match, the mechanism exists to reduce the profile of the LPA

even further. However, it is important to keep in mind that these materials have been assumed to be lossless, whereas the magnetic metamaterial will still have non-negligible losses. These materials have far less loss than naturally occurring magnetic materials, but a future research effort will have to focus on counteracting any degradation caused by introducing the loss characteristic to the model.

Another idealization made thus far is the use of an infinite flange. While this is a widely used mechanism in theoretical models, a practical application would require a minimal flange since the size of the aperture in absolute terms is still large at 2.1 ft^2. Before dedicating extensive time to improving the input impedance match for the S11 curve, we will verify that reducing the size of the flange does not negatively impact the results seen thus far.

2.7 Comparison of a Finite Flange to the Infinite Flange

Section 2.6 showed how increasing the permeability value of the μ_x tensor component of equation 4 further reduces the profile of the linearly tapered rectangular cavity. Since this improvement did not significantly degrade the performance of the LPA, this section will analyze the effect of surrounding the aperture with a finite flange. All the previous LPA models have assumed an infinite conducting flange surrounding the aperture. This is an idealization, and in practice an infinite flange or a large enough flange to approximate an infinite flange is not realistic at 200–500 MHz. Therefore, it is important to see how much the reduction in flange size will affect the results seen in section 2.6. The following results use the antenna dimensions listed in table 5 loaded with an anisotropic magnetic material with $\mu_x = 15$.

Figures 11a and 11b compare the results for a finite flange of 1 in surrounding the LPA aperture to those of the infinite flange presented in section 2.6. The blue curve represents the infinite flange and the red curve represents the finite flange. The figures show approximately a ±1.0 dB difference between the two realized gain curves and nearly identical S11 curves. This shows that even for a significant reduction in flange size, the LPA results achieve a comparable result, which is very important for real-life applications. The total size of the aperture plus the flange is now 2.4 ft^2. From now on, all results will be based on models using the 1-in flange.

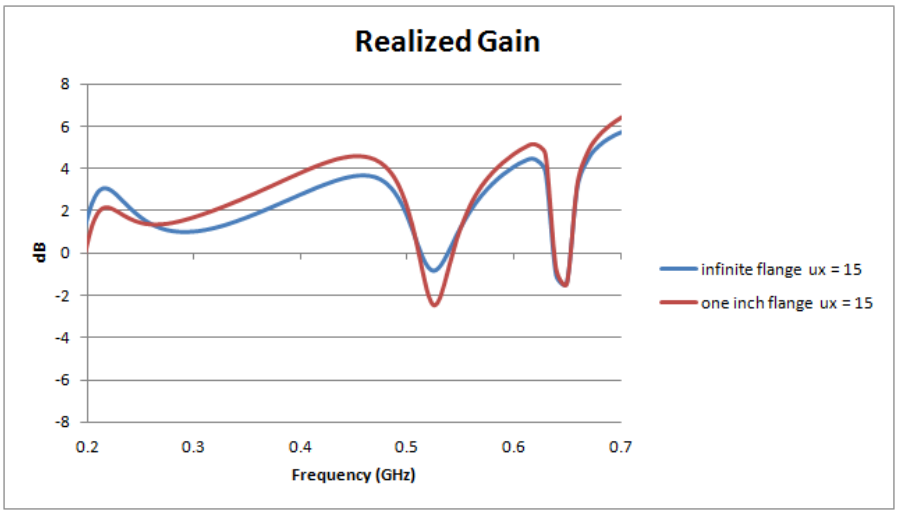

(a)

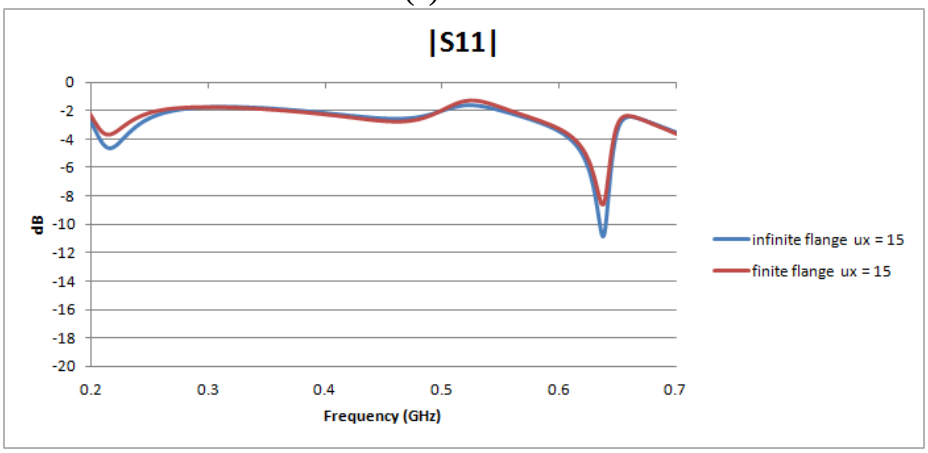

(b)

Figure 11. Simulation results of the model in figure 5a for an infinite flange and finite flange loaded with anisotropic magnetic material with μ_x = 15 for (a) realized gain and (b) |S11|.

Now that a suitable LPA design has been achieved with positive realized gain from 200 MHz–520 MHz, the focus will shift to achieving a better input impedance match. The first step in this process is to replace the linearly tapered rectangular cavity with a rectangular cavity shape based on the analytical solution to the transverse resonance condition for a partially loaded rectangular cavity.

2.8 Rectangular Cavity Derived from the Isotropic Transverse Resonance Condition

Sections 2.3–2.7 have shown various iterations on the original idea for the LPA design described in section 2.2. The best design so far has yielded a profile of d = 3.26 in, or a 70% reduction in profile over the benchmark antenna in section 2.1.

A novel idea for a linearly tapered rectangular cavity was proposed in section 2.3 to suppress the high order resonances causing instabilities in the realized gain and VSWR of figures 4a and 4b. To this point, all resulting LPA models investigated have used the linearly tapered rectangular cavity suggested in section 2.3 to achieve the suppression of higher order resonances. While this approach has been effective in that regard, poor input impedance matches at the coaxial input to the rectangular probe results in an inefficient antenna that is undesirable in real-world applications. This may be improved by rigorously deriving the shape of the LPA cavity using the transverse resonance condition of a rectangular cavity.

An equation that describes the shape of the transverse resonance rectangular cavity has been derived in appendix A for the isotropic case. This will be used as an initial approximation to the anisotropic case. Figures 12a and 12b show the dimensions of the rectangular cavity width in terms of L_g. L_g represents the distance from the edge of the high index anisotropic material to the edge of the rectangular cavity in the x-direction for all points inside the rectangular cavity. The equation for L_g is

$$L_g = \frac{\lambda}{2\pi}\tan^{-1}\left[\frac{\sqrt{\frac{\mu_r}{\varepsilon_r}}}{\tan\left(\frac{\pi w}{\lambda}\sqrt{\mu_r\varepsilon_r}\right)}\right], \tag{5}$$

where w is the width of the high index anisotropic material in the rectangular cavity at depth z. The parabolic shape of the rectangular cavity shown in figure 12a, results from the replacement of μ_r and ε_r in equation 5 with the values of the dominant axis from equation 4, which is also based on the linear taper of the high index anisotropic material within the rectangular cavity. The shape is unique to the shape of the high index anisotropic material and will change as w changes. Depending on how good of an approximation the linearly tapered rectangular cavity was to the transverse resonance cavity illustrated in figures 12a and 12b, there may be a noticeable difference in the S11 seen at the coaxial input.

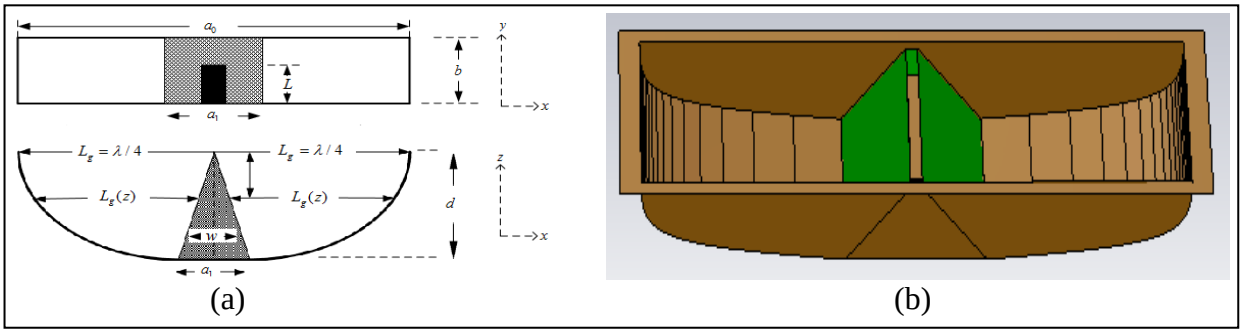

Figure 12. Illustration of (a) the geometry of the cavity derived from the transverse resonance condition and (b) the three dimensional view of the CST model.

Figures 13a and 13b compare the results for the shape of the transverse resonance cavity to those of the linearly tapered rectangular cavity. The dimensions of the LPA are the same as those listed in table 5. The blue curve represents the new results for the transverse resonance cavity, and the red curve shows the results for the linearly tapered cavity of the same dimensions and material loading. While the S11 curve does not show an improvement in the input impedance match at the lower frequencies, it does show a more flat S11 response above 400 MHz. This results in an increase in positive realized gain BW from 200 MHz–555 MHz, which represents a 180% BW. Again, there is the potential to extend the BW up to 675 MHz, which would represent a potential BW of 240%. The use of the transverse resonance rectangular cavity in the LPA design essentially improves the LPA performance to that of the linearly tapered rectangular cavity with the infinite flange. In order to reach the potential BW, the S11 from 550 MHz–575 MHz needs to be improved.

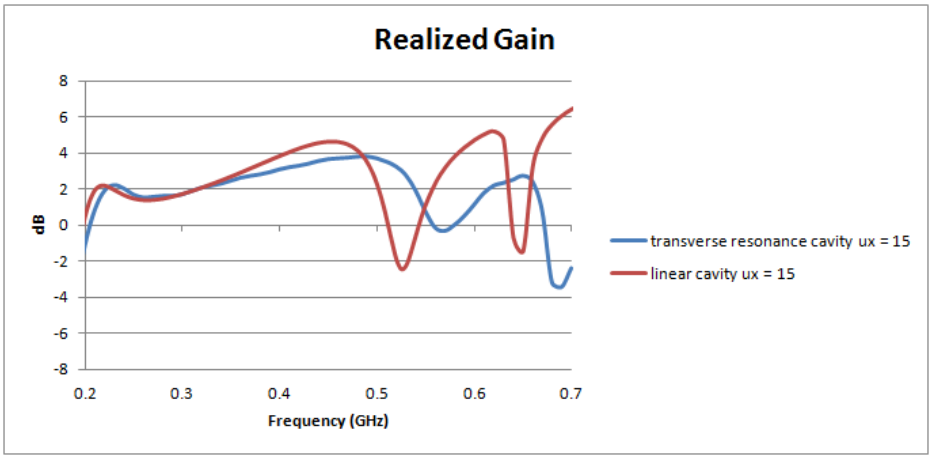

(a)

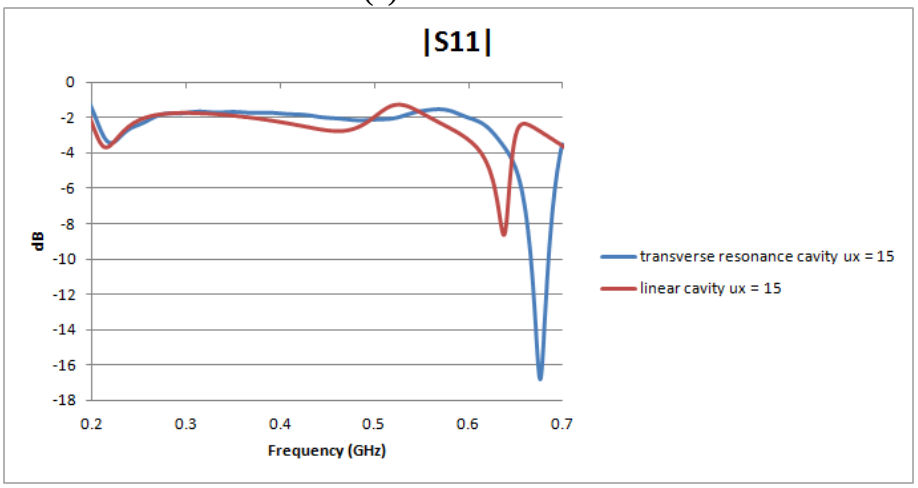

(b)

Figure 13. Simulation results of the model in figure 12a for the transverse resonance for (a) realized gain and (b) |S11|.

The minimal improvement in the performance of the LPA using the transverse resonance cavity over the linearly tapered rectangular cavity indicates that the linear taper was, in fact, a valid approximation to the actual transverse resonance cavity shape. Since a significant improvement in the S11 curve did not result, new methods of improving the input impedance match will be investigated in the next section.

2.9 Investigation of Probe Dimensions on S11 of the LPA

Currently, the design of the LPA has resulted in a profile of $0.055\lambda_r$ with a positive realized gain from 200 MHz–555 MHz. However, a poor S11 at the input of the probe keeps this design from achieving comparable results to the benchmark performance of the antenna with the air-filled rectangular cavity of section 2.1. One potential reason for this input impedance mismatch may stem from a reactance created within the cavity caused by the abrupt transition from high index metamaterial to free space near the aperture. One way to counteract this would be to change the width of the rectangular probe used to stimulate the fields inside the cavity. Thus far, all models have used $PW = 0.7$ in to match the width of the top of the load material. This section explores the effect that changing PW has on the S11 of the LPA at the coaxial input.

Figures 14a and 14b show the realized gain and S11 curves for different PW used to stimulate the field within the cavity. All other dimensions are the same as those listed in table 5 for $\mu_x = 15$. Figure 14b shows that as PW increases, there is better wideband performance for wider PW up to 8.0 in. When $PW = 10.0$ in, there is a degradation in the wideband performance. The best case scenario in terms of the impedance match is for when $PW = 8.0$ in. This provides a 175 MHz BW where the S11 is better than –10 dB from 400 MHz–575 MHz. This is a major improvement over a significant portion of the band.

Figure 14a shows how the realized gain is directly affected by this improvement in S11. There is up to a 4.0 dB improvement between the dark blue curve and purple curve representing the $PW = 0.7$ in and $PW = 8.0$ in cases respectively. A tradeoff in terms of realized gain has been made at the lower end of the frequency band to achieve this improved S11. The positive realized gain BW has now moved to 220 MHz–580 MHz. This corresponds to a 160% BW. However, the large improvement in realized gain and S11 over most of the band of interest represents the potential to further reduce the profile of the LPA if the S11 can be improved from 200 MHz–350 MHz.

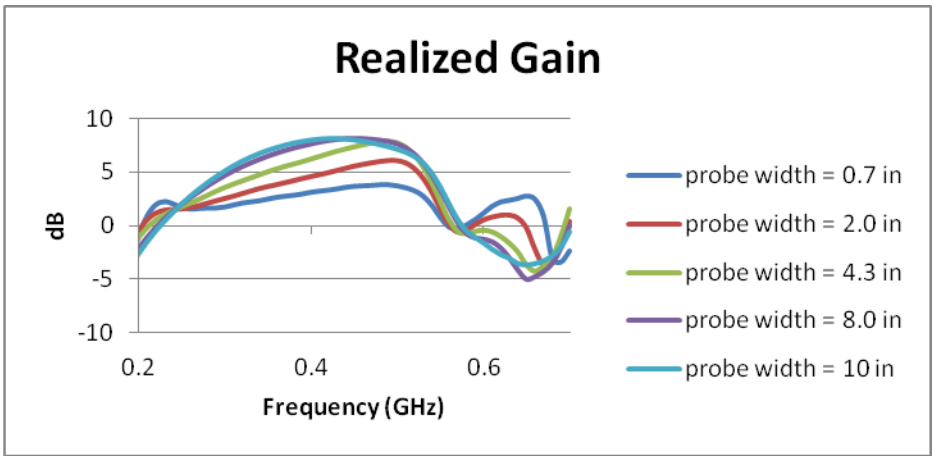

(a)

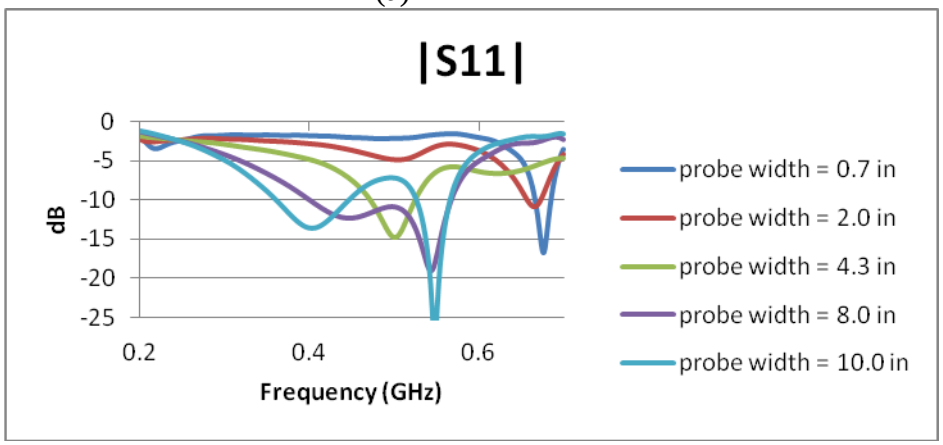

(b)

Figure 14. Simulation results of the model in figure 12a for different *PW* for (a) realized gain and (b) |S11|.

2.10 Comparison of LPA Design to Benchmark Antenna

Since section 2.8 demonstrates an improvement in S11 and also an improvement in realized gain, this LPA design marks the best achievement as far as this investigation has gone. In order to categorize how well this LPA performs a direct comparison of the results of section 2.8 to the benchmark antenna of section 2.1 are made. The antenna dimensions for both cases are listed in table 6. The blue curve corresponds to figures 14a and b, and the red curve corresponds to figures 2a and 2b.

Table 6. Dimensions in inches for the geometry of the transverse resonance cavity loaded with anisotropic μ_x = 15 material (blue) and the air filled rectangular cavity (red).

color	a_0	b	a_1	f_r (MHz)	d	δ	PW	L	h
blue	26.25	11.7	8.3	225	3.29	0.27	0.7	8.5	-
red	29.5	13.1	29.5	200	11.04	-	4.3	8.5	0.84

Figures 15a–c show the realized gain, S11, and VSWR curves for the transverse resonance cavity LPA versus the air-filled benchmark antenna of section 2.1. There is comparable performance from 350 MHz–550 MHz. Considering the profile of the LPA has been reduced from $0.19\lambda_r$ to $0.055\lambda_r$, where λ_r is calculated at 200 MHz, this represents a significant accomplishment. However, improvement is still needed to improve the S11 and realized gain from 200 MHz–350 MHz in the LPA design.

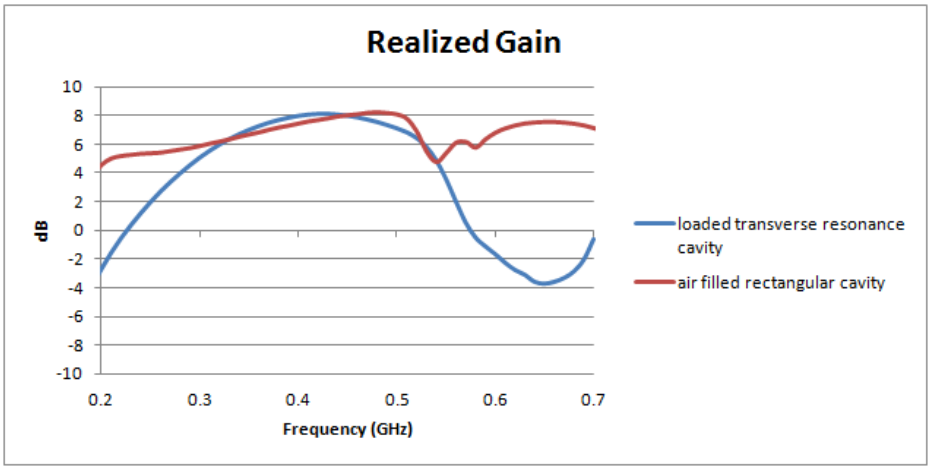

(a)

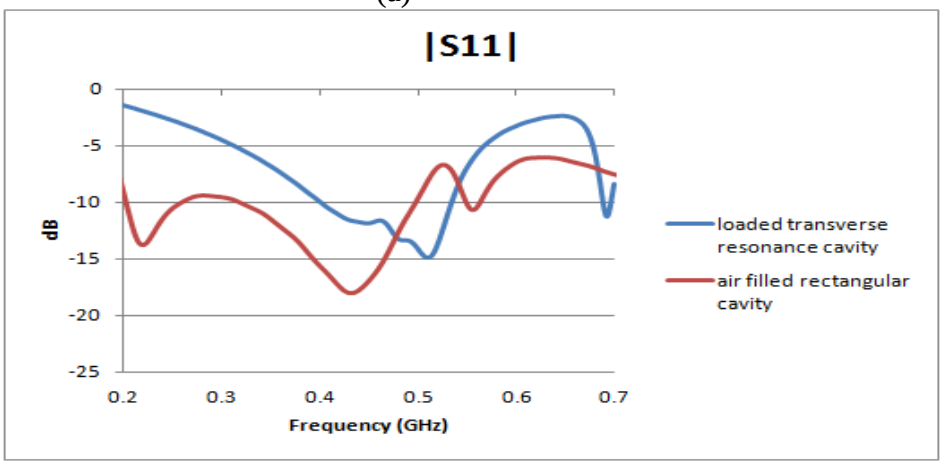

(b)

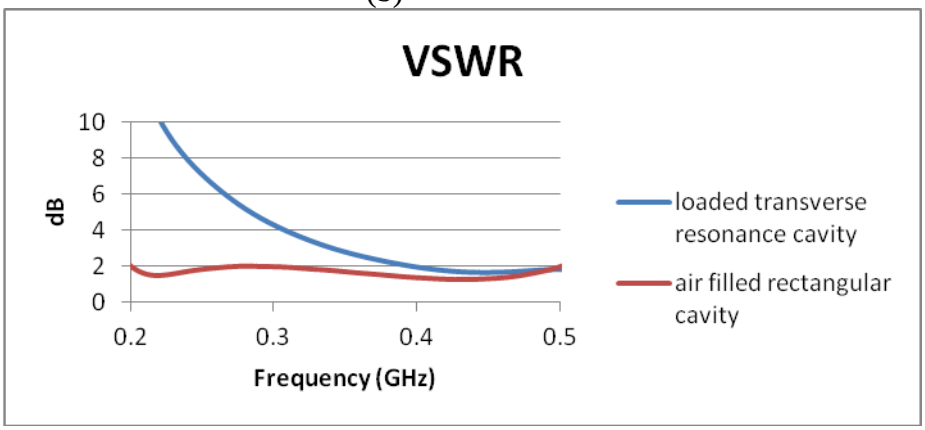

(c)

Figure 15. Simulation results of the model in figure 12a loaded with anisotropic $\mu_x = 15$ material and the model in figure 1a for (a) realized gain (b) S11, and (c) VSWR.

3. Conclusions

This report demonstrates the effects of profile reduction on a rectangular cavity-backed antenna by partially loading the cavity with anisotropic magnetic metamaterial. Research in this area has yielded a LPA design that has a profile of $d = 0.055\lambda_r$ at 200 MHz or, $d = 3.26$ in, with an aperture size of 2.4 ft^2 including a 1-in flange. This is a 70% reduction in total rectangular cavity profile compared to the $0.19\lambda_r$ case of $d = 11.04$ in. The LPA design has a positive realized gain from 220 MHz–580 MHz and a 3:1 VSWR from 350 MHz–575 MHz. This BW exceeds the design goals from 500 MHz–580 MHz but does not meet the design goals from 200 MHz–350 MHz. Further investigation into matching techniques is needed at the low frequencies to improve wideband performance of the LPA.

4. References

1. Wei Yan, Aixin Chen; Jiang, Tiehuq. Design of UHF Miniature Discone Antenna. *Proceedings of 9th International Symposium on Antennas Propagation and EM Theory (ISAPE)*, 2010.
2. Aixin, Chen; Jiang, Tiehua; Chen, Zhizhang; Su, Donglin; Wei, Wenxuan; Zhang, Yanjun. A Wideband VHF/UHF Discone-Based Antenna. *IEEE Antennas and Wireless Propagation Letters* **2011**, *10*.
3. Chen, A.; Jiang, T.; Chen, Z.; Su, D. A Novel Low-Profile Wideband UHF Antenna. *Progress in Electromagnetrics Research (PIER)* **2011**, *121*, 75–88.
4. Lagarkov, A. N.; Semeneko, V. N.; Kisel, V. N.; Christyaev, V. A. Development and Simulation of Microwave Artifical Magnetic Composities Utilizing Non-magnetic Inclusion. *Journal of Magnetism and Magnetic Materials* **2003**.
5. Maslovski, S.; Ikonen, P.; Kolmakov, I.; Tretyakov S. Artificial Magnetic Materials Based on the New Magnetic Particle Metasolenoid. *Progress in Electromagnetics Research (PIER)* **2005**, *54*, p. 61–81.
6. Baily, M. C. Broadband Half Wave Dipole. *IEEE Trans. On Antennas and Propagation* **April 1984**, *AP-32* (4).
7. Schelkunoff, S. A. Schelkunoff. *Electromagnetic Waves. DuHamelH* **1943**, *9*, Van Nostrand, New York.
8. Williamson, A. G..Analysis and Modeling of a Coaxial-line/Rectangular-waveguide Junction. *IEEE Proceedings (Microwaves, Optics, and Antennas)*, vol. 129, Issue 5. October 1982.
9. Wade, P. *Rectangular Waveguide to Coax Transition Design.* QEX, November/December 2006.
10. David Pozar. *Microwave Engineering*. 3rd. ed., John Wiley and Sons, 2005.

Appendix A. Derivation of a Tapered Rectangular Cavity Based on the Transverse Resonance Condition

This appendix outlines the derivation of an equation governing the shape of a tapered rectangular cavity for an antenna loaded with high index material. When loading the rectangular cavity with high index material, f_r is lowered and higher order resonances are introduced if a standard rectangular cavity is used.

To suppress these resonances, a linearly tapered rectangular cavity with a linearly tapered material shape can be used to maintain a more constant value of f_r, as shown in figure A-1. However, this is only an approximation to the actual shape the tapered rectangular cavity would take to maintain an exactly constant f_r.

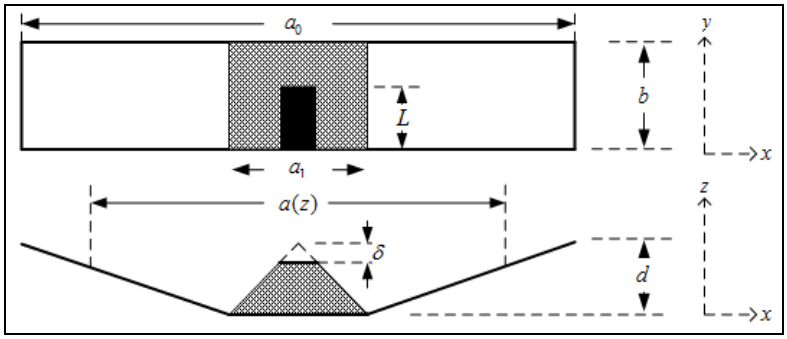

Figure A-1. Diagram of the linearly tapered rectangular cavity used to suppress higher order resonances.

To derive the shape that maintains an exact f_r, the transmission line model of the rectangular cavity depicted in figure A-2 is used. In figure A-2, both ends are shorted and the width of the high index material is distributed across the center. The shape of the rectangular cavity will be determined by determining the value of L_g for a given width of material w, which changes linearly as the rectangular cavity depth increases as depicted in figure A-1.

To start, the transverse resonance condition for admittance is (*10*)

$$\vec{Y}_{in} + \overleftarrow{Y}_{in} = 0 . \tag{A-1}$$

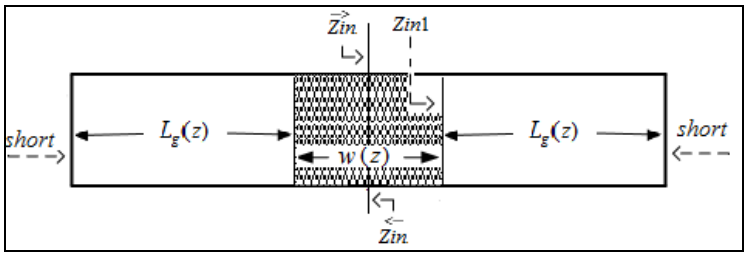

Figure A-2. Transmission line representation with either end shorted of the tapered rectangular cavity.

To satisfy this condition, the value of $\vec{Z}_{in}$ must be determined at the center of figure A-2. Due to symmetry, $\vec{Z}_{in}$ will be identical at this point looking in from either direction. For a short circuited load, $\vec{Z}_{in1}$ is

$$\vec{Z}_{in1} = j * Z_o \tan\left(\beta_o L_g\right), \tag{A-2}$$

where $\beta_o = \omega\sqrt{\mu_o \varepsilon_o}$ and $Z_o = \sqrt{\frac{\mu_o}{\varepsilon_o}}$. Now use the equation for input impedance to determine the value of $\vec{Z}_{in}$ as

$$\vec{Z}_{in} = Z_e \left[\frac{Z_{in1} + jZ_e \tan\left(\beta_e \frac{w}{2}\right)}{Z_e + jZ_{in1} \tan\left(\beta_e \frac{w}{2}\right)} \right], \tag{A-3}$$

where $\beta_e = \beta_o \sqrt{\mu_r \varepsilon_r}$ and $Z_e = Z_o \sqrt{\frac{\mu_r}{\varepsilon_r}}$. The symmetry of the transmission line in figure A-2 allows us to rewrite the transverse resonance condition in equation A-1 as

$$2\vec{Y}_{in} = 0, \tag{A-4}$$

where $\vec{Y}_{in} = \frac{1}{\vec{Z}_{in}}$. To satisfy equation A-4, set the denominator of equation A-3 to zero such that

$$Z_e - Z_o \tan\left(\beta_o L_g\right) \tan\left(\beta_e \frac{w}{2}\right) = 0, \tag{A-5}$$

Now divide out Z_o to arrive at the following expression

$$\sqrt{\frac{\mu_r}{\varepsilon_r}} - \tan\left(\beta_o L_g\right) \tan\left(\beta_e \frac{w}{2}\right) = 0. \tag{A-6}$$

Solving equation A-6 for L_g and normalizing by λ yields the following equation for L_g

$$\frac{L_g}{\lambda} = \frac{1}{2\pi}\tan^{-1}\left[\frac{\sqrt{\frac{\mu_r}{\varepsilon_r}}}{\tan\left(\frac{\pi w}{\lambda}\sqrt{\mu_r \varepsilon_r}\right)}\right]. \qquad \text{(A-7)}$$

Equation A-7 will define the shape of the tapered rectangular cavity versus the width of the high index material at all points inside the cavity.

Plotting L_g versus w for a magnetic material (μ_r = 10, ε_r = 1) yields the plot of the walls of the tapered rectangular cavity, as depicted in figure A-3.

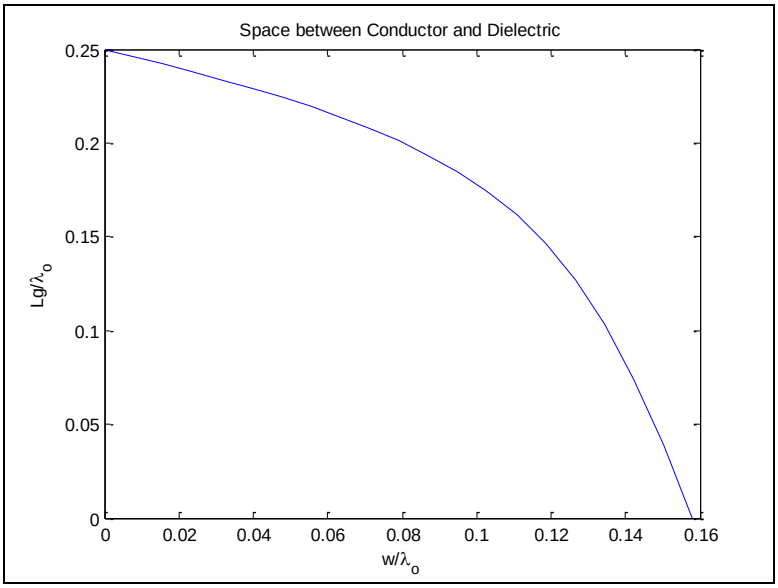

Figure A-3. Plot of L_g versus w for a magnetic material.

1	DEFENSE TECH INFO CTR
(PDF)	ATTN DTIC OCA
2	US ARMY RSRCH LABORATORY
(PDF)	ATTN IMAL HRA MAIL & RECORDS MGMT
	ATTN RDRL CIO LL TECHL LIB
1	GOVT PRNTG OFC
(PDF)	ATTN A MALHOTRA
5	US ARMY RSRCH LAB
(PDF)	ATTN RDRL SER M A ZAGHLOUL
	ATTN RDRL SER M E ADLER
	ATTN RDRL SER M G MITCHELL
	ATTN RDRL SER M S WEISS
	ATTN RDRL SER M W O COBURN